ELSEVIER

International Journal of Heat and Fluid Flow 23 (2002) 242–257

International Journal of HEAT AND FLUID FLOW

www.elsevier.com/locate/ijhff

Interface tracking towards the direct simulation of heat and mass transfer in multiphase flows ☆

D. Lakehal *, M. Meier, M. Fulgosi

Institute of Energy Technology, Swiss Federal Institute of Technology Zurich, ETH-Zentrum/CLT, CH-8092 Zurich, Switzerland

Abstract

The paper presents recent trends in the development of prediction methods for the direct numerical simulation of multiphase flows based on the one-fluid formalism coupled with various interface tracking algorithms. The methods are based on solving a single set of transport equations for the whole computational domain and treating the different phases as a single fluid with variable material properties. Changes in these properties are accounted for by advecting a phase indicator function. Interfacial exchange terms are incorporated by adding the appropriate sources as delta functions or smoothed gradients of the composition field at or across the interface. The strategies are first discussed within the isothermal phase context and then for situations featuring inter-phase heat and mass transfer. Various aspects such as the treatment of capillary forces are discussed, supported by selected examples demonstrating recent progress drawn from the current work of the authors. © 2002 Published by Elsevier Science Inc.

Keywords: Multiphase flow; One-fluid formulation; Volume of fluid; Level sets; Boundary fitting; Heat and mass transfer

1. Introduction

Multiphase flows appear in natural and industrial processes in various forms, often featuring inter-phase heat and mass transfer. Examples include evaporating dispersed phases in the natural environment or in combustion chambers, condensation of steam in power production components, erosion over wings and blades, liquid metal sprays, transfer of soluble gases at the atmosphere–ocean interface, among others. At present, there is a considerable ongoing effort directed towards clarifying inter-phase transfer mechanisms at moving interfaces using direct computational methods, without use of models. This will not be possible for all types of multiphase flows, but for the class of flow in which the phases can be clearly distinguished from each other, (see, for example, Fig. 1). The interest in these new methods is dictated by the fact that earlier, well-established averaging-based models have often not been capable of generating accurate solutions in the engineering sense.

Solving the Navier–Stokes equations governing the motion of multiple phases for the simulation of real problems has proven to be complex. This explains the relatively slow progress of this discipline as compared to classical computational fluid dynamics applied to single-phase flows. What makes *computational multiphase science* particularly challenging is the variety of phenomena in which the phases interact: Pollutant or spray dispersion has little in common with stratified pipe-flows, and almost none with spinodal decomposition of a binary fluid. The way of predicting CO_2 absorption by oceans differs from the strategy for handling evaporating droplets over waves, although both phenomena are closely related. Thus, prediction strategies have to be tailored for specific goals and research in this field has to be variable in its approach.

Central to the numerical simulation of multiphase flows is the accurate identification of interface dynamics through which flow regimes can be defined and associated inter-phase transfer mechanisms can be quantified. In present modelling strategies phenomena taking place at the interface separating phases are either modelled within the framework of the *interpenetrating-continua* approach, also known as the *two-fluid* method (see, for

☆ This paper is a revised and expanded version of a paper presented at CHT'01, the Second International Symposium on Advances in Computational Heat Transfer (Palm Cove, Qld., Australia, 20–25 May 2001), the proceedings of which were published by Begell House, Inc.

* Corresponding author.
E-mail address: lakehal@iet.mavt.ethz.ch (D. Lakehal).

0142-727X/02/$ - see front matter © 2002 Published by Elsevier Science Inc.
PII: S0142-727X(02)00172-8

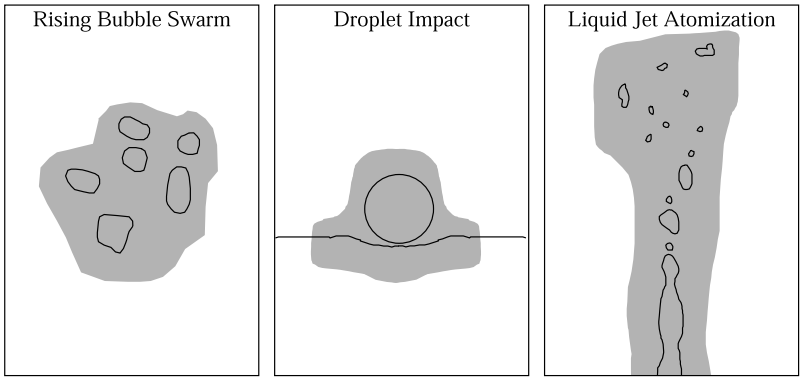

Fig. 1. Examples of flows within reach of *interface tracking* methods.

example, Ishii, 1975), or the topology and dynamics of the interface are directly simulated by use of direct *interface tracking methods* (ITM). In the averaged *two-fluid* formalism, each point in the mixture is occupied simultaneously (in variable proportions) by both phases, and separate conservation equations are required for each field. The problem here is the specification of closure laws for interfacial mass, momentum and energy exchanges, and the corresponding interfacial area. Furthermore, the evolution of the volumetric interfacial area is predicted using an additional transport equation (see, for example, Morel et al., 1999), in which the mechanisms driving flow-regime transitions and relaxation times associated with these can be taken into account in a mechanistic way.

ITM are supposed to be applied in the opposite scenario, i.e. when the identification of interfaces needs to be precise, for example in the breakup of large bubbles, for droplets or liquid jets, in crystal growth, flame propagation, or hydrodynamic instability formation (see, for example, Fig. 1). The key to these methods is the use of a single-phase set of conservation equations, known as the *one-fluid* formulation, where the differences in material properties and surface tension are accounted for by solving a convection equation for the composition or phase indicator field. The concept is attractive, since it offers the prospect of a more subtle and precise strategy for the exact identification of interfaces than the *two-fluid* formulation. Thus, in contrast to the average model, interface tracking approaches avoid resorting to empiricism to predict interfacial physics driving the flow.

Compared with the *interpenetrating-continua* formulation, the interface tracking approach can be thought of as a direct numerical simulation (DNS) of interface motion (not of turbulence), where no closure assumptions for the interfacial area evolution are needed. In the case where the flow is turbulent, the stresses are either modelled within the framework of the RANS approach, or else the turbulent structures down to the Kolmogorov scales are directly simulated by reference to conventional DNS of turbulence. Combining DNS of turbulence with ITM for the prediction of turbulent two-phase flows is not practical, because the computational costs for simulating turbulent flows increase with Reynolds number, and both the accuracy and stability of the numerics deteriorate with increasing complexity of the interfacial topology. This *super DNS of two-phase flows* is understandably limited to a narrow range of applications, where it can only serve as a sophisticated numerical experiment for exploring small-scale, turbulence-related phenomena at the interface.

The present paper aims at addressing selected ITM for the prediction of the class of multiphase flow where surface tension forces are important. The focus is on the predictive performance of these methods, on the difficulties encountered when extending them to flow configurations featuring strong topological changes, and on recent variants and modifications. The work is complemented by the presentation of a related method, capable of directly predicting turbulence over a deformable interface without modelling, i.e. *super DNS of two-phase flows*.

2. Beyond the two-fluid formulation

The *interpenetrating-continua* approach is generally employed when the exact shape of the interface is not known, or not relevant. The main problem with this strategy, and with all other methods based on ensemble averaging, is the crucial need for the specification of closure laws for interfacial exchanges. Only in certain very simple cases, such as horizontal stratified flows featuring slugs, smooth annular flows, waves, or spherical drops and bubbles, can the shape of the interface be easily identified and modelled. For more complex flow regimes, including those where surface tension plays a role, the shape and evolution of the interfaces are not easily definable, and this explains the interest in developing ITM. First applications of these techniques focus on the prediction of interfacial motions in relatively

simple cases, such as the stability of inclusions of one phase inside another, as in the breakup of large bubbles, droplets, or liquid jets (Fig. 1).

2.1. The continuity equation for the one-fluid formulation

The exact, or microscopic instantaneous equations governing two-phase flow systems can formally be written in terms of the *component indicator function*, or the composition field, $\chi_k(\mathbf{x},t)$, at time t and point $\mathbf{x}$, defined by $\chi_k(\mathbf{x},t)=1$ for $\mathbf{x}\in$ phase k, and $\chi_k(\mathbf{x},t)=0$ otherwise. Since χ_k is a property moving with the flow, its material derivative is obviously zero (Drew and Passman, 1999)

$$\frac{D\chi_k}{Dt}=\frac{\partial\chi_k}{\partial t}+\mathbf{u}\cdot\nabla\chi_k=0. \tag{1}$$

This is known as the *topological equation* describing the motion of a surface marked with χ_k, moving with velocity $\mathbf{u}$. Note in particular that this is a weak formulation of the problem since the discontinuity of χ_k (across interfaces) makes it a non-derivable function.

In the absence of heat and mass transfer, the mass balance equation for two non-miscible, contacting phases (for example, L for liquid and G for gas) contained within volume V as shown in Fig. 2 can be written as

$$\chi_L\frac{\partial\rho_L}{\partial t}+\chi_L\nabla\cdot(\rho_L\mathbf{u})=0, \tag{2}$$

$$(1-\chi_L)\frac{\partial\rho_G}{\partial t}+(1-\chi_L)\nabla\cdot(\rho_G\mathbf{u})=0, \tag{3}$$

where ρ_L denotes the liquid density and ρ_G the gas density. The above system of equations can be reformulated in a more convenient form

$$\frac{\partial}{\partial t}(\chi_L\rho_L)+\nabla\cdot(\chi_L\rho_L\mathbf{u})=\rho_L\frac{D\chi_L}{Dt}=0, \tag{4}$$

$$\frac{\partial}{\partial t}[(1-\chi_L)\rho_G]+\nabla\cdot[(1-\chi_L)\rho_G\mathbf{u}]=-\rho_G\frac{D\chi_L}{Dt}=0. \tag{5}$$

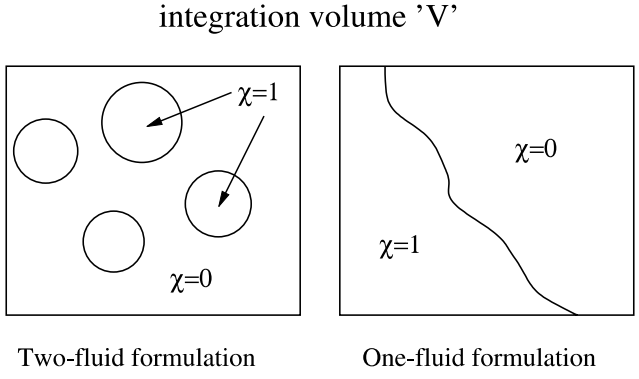

Fig. 2. Examples of integration volumes used for describing multiphase flow systems.

Within the *two-fluid* formulation, Eqs. (4) and (5) are first appropriately averaged (for example, over volume, as shown in Fig. 2(left)). They are then solved simultaneously, together with the momentum and energy equations for each phase. In the *one-fluid* variant, however, the above set of equations can be combined in a way leading to a single conservation equation but with variable density ρ dictated by the interface location. This is obtained by combining Eqs. (4) and (5)

$$\frac{\partial\rho}{\partial t}+\nabla\cdot(\rho\mathbf{u})=0 \quad \text{with } \rho=\rho_G+(\rho_L-\rho_G)\chi_L. \tag{6}$$

Using Eq. (1) and taking $\partial_t\rho_L$ and $\partial_t\rho_G$ to be identically zero for incompressible fluids simplifies this equation to

$$\frac{\partial\chi_L}{\partial t}+\mathbf{u}\cdot\nabla\chi_L+\frac{\rho}{(\rho_L-\rho_G)}\nabla\cdot\mathbf{u}=0 \tag{7}$$

which finally reduces to the form below

$$\nabla\cdot\mathbf{u}=0. \tag{8}$$

This result is important since in certain Navier–Stokes solvers based on the finite volume approach Eq. (8) is generally written as $\nabla\cdot\rho\mathbf{u}=0$, which obviously is not compatible with Eq. (6).

2.2. The one-fluid formulation for flows with capillary forces

To account for appreciable density and viscosity jumps across an interface separating two non-miscible phases the *one-fluid* method (Kataoka, 1986) presents itself as a natural alternative. Here, both phases are treated by a single set of conservation laws for the entire flow field, but the differences in the material properties of the phases and capillary forces (when appropriate) are explicitly accounted for. In this case the local balance equations for incompressible, Newtonian fluids are written as

$$\nabla\cdot\mathbf{u}=0, \tag{9}$$

$$\frac{\partial\rho\mathbf{u}}{\partial t}+\nabla\cdot(\rho\mathbf{u}\mathbf{u})=-\nabla p+\nabla\cdot\tau+\rho\mathbf{g}+\gamma\nabla\cdot\mathbf{\Phi}, \tag{10}$$

$$\frac{\partial\rho E}{\partial t}+\nabla\cdot(\rho E\mathbf{u})=\nabla\cdot(k\nabla T)+(-pI+\tau+\gamma\mathbf{\Phi}):\nabla\mathbf{u}, \tag{11}$$

where $\mathbf{g}$ stands for the acceleration of gravity, p for the pressure, E for the internal energy, T for the temperature, k for the heat conductivity, $\tau=\mu(\nabla\mathbf{u}+\nabla\mathbf{u}^T)$ denotes the viscous stress tensor, with μ representing the dynamic viscosity, and $\mathbf{\Phi}$ is the capillary stress, with γ being the coefficient controlling the strength of the capillary forces. In these equations, material properties such as the density depend locally on the phase indicator function χ_k determined by use of the topological Eq. (1)

$$\eta(\chi,t)=\eta_{\mathrm{G}}+(\eta_{\mathrm{L}}-\eta_{\mathrm{G}})\chi_{\mathrm{L}}. \tag{12}$$

Note that this is not true for the viscosity for which the above relation can only be utilized as a model.

The capillary tensor $\mathbf{\Phi}$ represents the energy concentrated at a diffuse interface because of the prevailing density or composition field gradient $\nabla\chi$ (Anderson et al., 1998). It reflects the rate of change of the fluid's free energy density ξ with respect to the composition field χ, i.e. $\mathbf{\Phi}=\delta\xi/\delta\chi$. The conditions under which this generalized form of capillary tensor can be reduced to the conventional and simplified surface tension model are discussed below.

The capillary tensor (in fact, the free energy density) is a function not only of the thermodynamic properties such as the density, but also of their gradients. As defined by Anderson et al. (1998), Nadiga and Zaleski (1996), Chella and Vinals (1996), this tensor has the form

$$\mathbf{\Phi}=\left(\chi\nabla^2\chi+\frac{1}{2}|\nabla\chi|^2\right)I-\nabla\chi\otimes\nabla\chi \tag{13}$$

with I denoting the identity matrix and $\otimes$ a tensor product. Moreover, it can be shown that

$$\nabla\cdot\mathbf{\Phi}=\chi\nabla\left(\nabla^2\chi\right). \tag{14}$$

This particular form of the capillary tensor is derived from the simplest model of free energy density ξ due to van der Waals (1893). Jacqmin (1999) employs yet a slightly different form for ξ and thus for $\mathbf{\Phi}$, in which relation (13) appears as a particular case under hypothesized conditions. Methods using the form of capillary forcing given by Eq. (13) combined with the Navier–Stokes equations are known as *diffuse-interface* models (Anderson et al., 1998; Jacqmin, 1999). A detailed description of the system of equations governing the motion of binary viscous fluids is given by Lowengrub and Truskinovsky (1998), who referred to it as the Navier–Stokes-Cahn–Hilliard (NSCH) model. They have been widely employed in applications where capillary forces were particularly dominant, e.g. in spinodal decomposition by Anderson et al. (1998), Jacqmin (1999), and Verschueren et al. (2001).

Chella and Vinals (1996) demonstrated that in the limit of smoothly curved, thin interfaces, and when the interface motion is slow compared with the local relaxation time of χ, the capillary source term appearing in Eqs. (10) and (11) can be approximated by

$$\gamma\nabla\cdot\mathbf{\Phi}\approx-|\nabla\chi|^2K\kappa\mathbf{n}, \tag{15}$$

where $\mathbf{n}$ denotes the unit vector normal to the interface, K is a positive constant, and κ represents the local curvature defined by

$$\kappa=-\nabla\cdot\mathbf{n}=-\nabla\cdot\left(\frac{\nabla\chi}{|\nabla\chi|}\right). \tag{16}$$

Integrating Eq. (15) over the interfacial area (ds) yields the *continuous surface force* (CSF) model of Brackbill et al. (1992)

$$\int\sigma\kappa\delta(\mathbf{x}-\mathbf{x_f})\mathbf{n}\,\mathrm{d}s, \tag{17}$$

where σ is the surface tension, assumed to be constant across the entire thickness of the interfacial sublayer, and $\delta(\mathbf{x}-\mathbf{x_f})$ represents a Dirac pulse with $\mathbf{x}_f$ being the instantaneous location of the interface. The delta function appears in the above expression because use was made of

$$\nabla\chi=\int\delta(\mathbf{x}-\mathbf{x_f})\mathbf{n}\,\mathrm{d}s. \tag{18}$$

The surface tension σ reflects the excess of capillary energy concentrated at the interface per unit surface area caused by the variation in χ across the interfacial sublayer.

In order to avoid having to deal explicitly with the curvature, a further manipulation of Eq. (13) led Lafaurie et al. (1994) and Scardovelli and Zaleski (1999) to the following anisotropic variant of the CSF-based capillary forcing:

$$\int\sigma\kappa\delta(\mathbf{x}-\mathbf{x_f})\mathbf{n}\,\mathrm{d}s\equiv\sigma\nabla\cdot\left(|\nabla\chi|I-\frac{\nabla\chi\otimes\nabla\chi}{|\nabla\chi|}\right) \tag{19}$$

also known as the *continuous surface stress* (CSS) model. Both CSF and CSS are in principle simple, robust and require only the phase field χ to be determined. However, both are also known to induce spurious currents near the interface, because once discretized, the exact momentum jump condition at the interface is not always properly preserved, i.e. pressure and viscous stress forces do not balance the capillary forces. This is partly due to the lack of precision in solving the curvature, but it also results from the way the surface term is discretized in the momentum equations. But even so, the CSF model and its variants have been attractive to various researchers (Kothe and Mjolsness, 1992; Kothe et al., 1996; Richards et al., 1995; Rider et al., 1995) essentially because of their simplicity of implementation. The composition field in diffuse-interface models is employed as a mass concentration field with its proper thermodynamic law for chemical diffusion. It therefore requires either predefined (known) thermodynamics for the composition field (or density), or the topological equation for the composition field [1] involves a fourth-order derivative of χ^{k} accounting for the thermodynamics for chemical diffusion in question. The model has not yet been

[1] In applying their *second-gradient* theory for the Stefan problem, which is a sort of *diffuse-interface* model, Jamet et al. (2001) employed the exact, one-dimensional solution for the density profile across a plane liquid–vapour interface. Therefore, they did not solve for the topological Eq. (1).

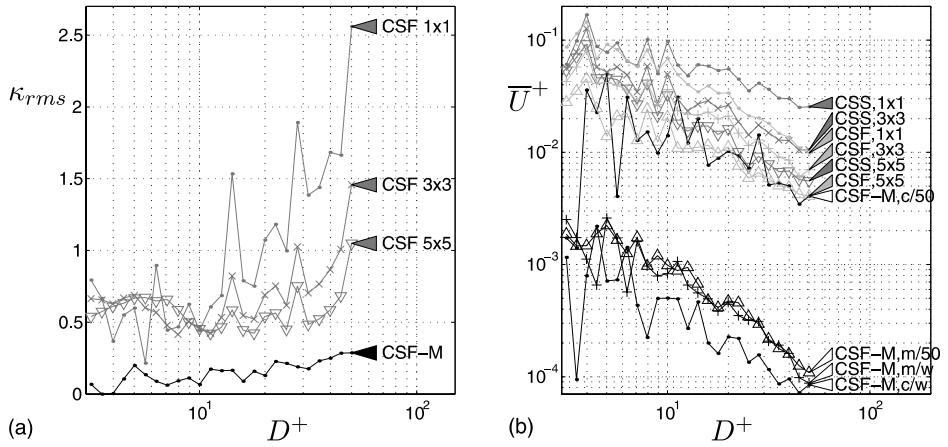

Fig. 3. (a) Standard deviations of the normalized curvature estimates κ vs. normalized diameter $D^+ = D/\Delta x$ obtained using Meier's et al. method (labelled CSF-M), for various smoothing matrices, 1×1, 3×3 and 5×5; (b) normalized mean (induced by parasitic currents) velocity $\overline{U}^+$ in the entire domain vs. D^+.

compared to CSF and CSS in terms of generation of spurious currents.

2.3. Performance and impact of CSF-based models

To alleviate some of the drawbacks associated with the CSF approach, Meier et al. (2002) developed a new technique for determining the curvature κ and for including the surface-tension source term in a way that keeps spurious currents low (referred to as CSF-M). In their approach, the curvature is determined more accurately by means of an estimator function fitted with a least-squares-fit against reference data, and the surface tension force is discretized so as to considerably reduce parasitic currents. The method was found to minimize these currents when employed together with a specific algorithm for interface reconstruction as discussed within the context of Fig. 3.

The benchmark problem considered refers to the distribution of surface tension around a circular droplet, where curvature is nominally known and constant. A spectrum of 25 droplets with variable diameters D^+ (normalized by Δx) was specified. Fig. 3 compares the results of this new method, CSF-M, with those obtained using CSF and CSS, Eqs. (17) and (19), respectively. The resulting standard deviations of κ and the mean velocity estimates over the entire domain are shown in Fig. 3(a). This reveals a high level of noise in the curvature estimates obtained using CSF, whereas Meier's et al. CSF-M approach achieved about three to seven times better agreement of the mean curvature with the reference value, and an approximately four to seven times lower standard deviation. Moreover, in comparison with the other two methods the CSF-M approach reduces by two to three orders of magnitude the spurious currents reflected by the artificial mean velocity around the bubble (Fig. 3(b)).

As validation exercises Meier et al. (2002) performed a number of tests with use of their modified CSF-M method, including rising bubbles in the six different regimes identified by Clift et al. (1978), and breakup of a liquid jet (more details can be found in Meier, 1999). In these, different bubble shapes can be distinguished as a function of the Eötvös and Morton numbers, defined respectively by $Eo = g\Delta\rho D^2/\sigma$ and $M = g\mu^4\Delta\rho/\rho^2\sigma^3$, with D being the diameter of a sphere of equal volume. Fig. 4 shows computation results of Meier et al. (2002) obtained with CSF-M. In that simulation, an axisymmetric grid containing 35×175 cells was employed. Comparison with the experimental map regime proposed by Clift et al. (1978) shows a remarkable agreement in the shape of bubbles. With use of the CSF model, however, the bubbles were found to experience non-physical fragmentation. Apart from this, certain quantitative measures (aspect ratio for case 3, wake angle in case 6) were found to compare reasonably well with the data.

3. Interface tracking methods: classification

The most frequently employed Eulerian-based [2] ITM for predicting certain classes of multiphase flows are the volume of fluid (VOF) method (Hirt and Nichols, 1981; Kothe and Mjolsness, 1992; Kothe et al., 1996; Richards et al., 1995; Rider et al., 1995; Rider and Kothe, 1998), the front tracking (FT) or immersed boundary method (Juric and Tryggvason, 1998; Unverdi and Tryggvason, 1992), the level set (LS) methods (Fedkiw et al., 1999; Osher and Sethian, 1988; Osher and Fedkiw, 2001;

[2] This means that the grid is always fixed independently of the way the interface is identified. This distinguishes from Lagrangian methods in which the grid moves with the interface.

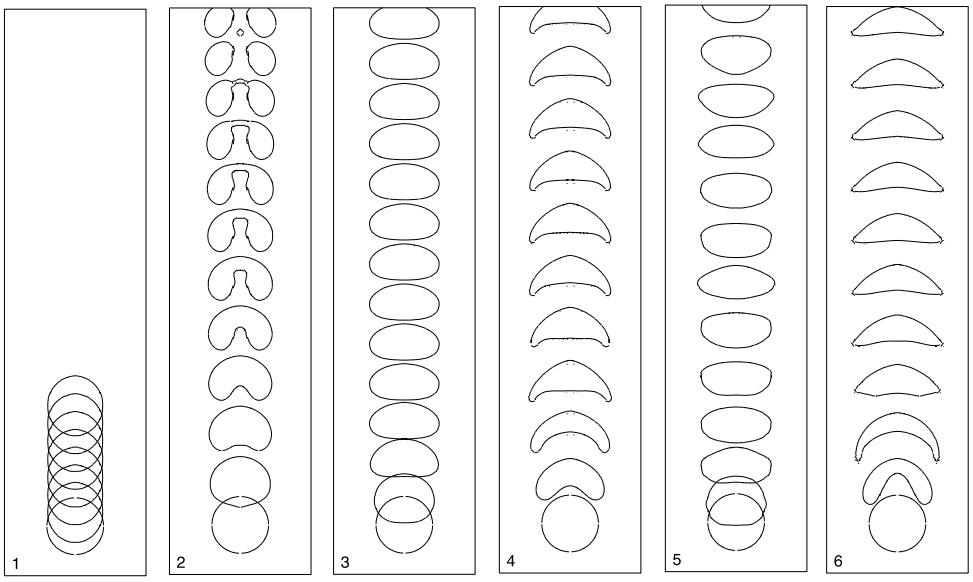

Fig. 4. Rising bubbles in different regimes. Data taken from Meier (1999) and Meier et al. (2002).

Sussman and Smereka, 1997), and the phase field (PF) methods (Anderson et al., 1998; Jacqmin, 1999; Lowengrub and Truskinovsky, 1998). The boundary fitting method (De Angelis, 1998; Fulgosi et al., 2001) is not of practical use; it can be better employed as a DNS for idealized flows. What is important to note is that in these methods the location of the interface is obtained by inspecting the phase indicator function $\chi(\mathbf{x}, t)$, which has a particular physical meaning in each approach. The FT approach differs from the others because it employs discrete (marker) points to localize the interface rather than continuous functions. This method is not treated in the present work. In a further classification the interface sublayer separating the phases is predicted by the use of VOF as being massless and of zero thickness. The other methods assume, however, diffuse interfaces, a property shared by all FT schemes.

4. The volume of fluid method

4.1. Basic formalism

The VOF approach relies on the definition of the *liquid volume-fraction* field or the volumetric proportion occupied by one of the phases within volume V (Fig. 2(right)). This fluid property is conventionally denoted (in a discrete from) by F_{ij} and defined by

$$F_{ij} = \frac{1}{V}\int_V \chi(\mathbf{x}, t)\,\mathrm{d}V, \tag{20}$$

where in this context V is the cell volume. In the VOF context, Eq. (1), therefore, represents the evolution of the *liquid volume-fraction*, identifying flow regions containing pure liquid (where $F_{ij} = 1$) from pure gas flow regions (where $F_{ij} = 0$). Interfacial cells are such that $0 < F_{ij} < 1$. The VOF method does not amount solely to the solution of Eq. (1); it requires accurate algorithms for advecting the volume fraction function so as to preserve conservation of mass. Since this cannot be achieved by means of conventional finite-difference schemes because of numerical diffusion, the composition field is first advected, after which the interface location is reconstructed to avoid numerical smearing of the interface. Briefly, updated interface information (after a convection step of Eq. (1)) is discarded in favor of the discrete volume fraction F_{ij}. The interface geometry is instead inferred, and its location is *reconstructed* from local volume fraction data using an appropriate algorithm. Once this type of algorithm is applied for advecting the volume fraction, the mass is systematically conserved even if the interface remains sharp. The reconstructed interface is then used to determine weighted cell material properties according to Eq. (12), for example. The disadvantage of having sharp inter-phase transitions in the volume fraction field is that the curvature κ can be highly oscillatory even for perfectly round surfaces. This could probably be avoided if curved interface reconstructions were used instead of line-segment reconstructions.

Earlier reconstruction schemes, usually called simple line interface construction (SLIC), used only vertical or horizontal lines in each cell to reconstruct interfaces (Noh and Woodward, 1976). More recently, reconstructions such as the piecewise linear interface construction (PLIC) method, employ straight, oblique lines in each cell (Rider et al., 1995; Rider and Kothe, 1998). This has several advantages: Fluid properties can be

allocated more accurately, and so can the interface area, enabling a more realistic implementation of surface tension and interfacial transfer models. In the meantime, new reconstruction algorithms have appeared recently using splines and quadratics.

4.2. Illustrative examples

4.2.1. Collapsing cylinder of water

Interface tracking-based incompressible flow solvers can be very well tested with dam-break problems. A volume of liquid kept back behind a dam is released by suddenly removing this barrier. In most experiments reported in the literature, a geometry suitable for two-dimensional, Cartesian simulations is used. Munz and Maschek (1992) instead performed an experiment with cylindrical symmetry, which makes it particularly useful for validating axisymmetric codes.

In the experiment, a cylindrical column of water of diameter 110 mm and height 200 mm was released by suddenly lifting the tube which had kept back the water. The water spread radially on the flat bottom to the side wall of the pot, where it sloshed upwards, fell back and collapsed back to the centre where a jet shot up. Up to this secondary collapse, the flow was fairly axisymmetric, smooth and laminar, thus, prediction with an axisymmetric, laminar flow simulation should be possible. However, during the secondary collapse, with growing asymmetries, this sort of idealization is bound to fail. The test case was simulated with the PLIC–VOF method by Meier (1999), using 50×80, 100×160 and 150×240 cells, respectively. Surface tension was neglected since it should be of importance only during and after the secondary collapse. Resulting interface shapes corresponding to the movie images are shown in Fig. 5. The main features of the flow are shown to be well simulated, including collapse, radial spreading, sloshing on the side wall and secondary collapse. The formation of a "crown" on the top and the main interface shape at $t = 0.08$ and 0.2 s is also well reproduced. The collapse of the crown leads to a thin central upward jet at $t = 0.38$ s; this is again a (minor) overprediction due to the flow symmetry imposed in the simulation. At $t = 0.52$ and 0.7 s, where the flow loses its spatial symmetry, the main shapes are still reasonably well reproduced. The characteristic times, heights and run-out lengths were also well reproduced (see, Meier, 1999). But because the simulation imposes symmetry on the flow, the predicted central sloshing heights were overestimated.

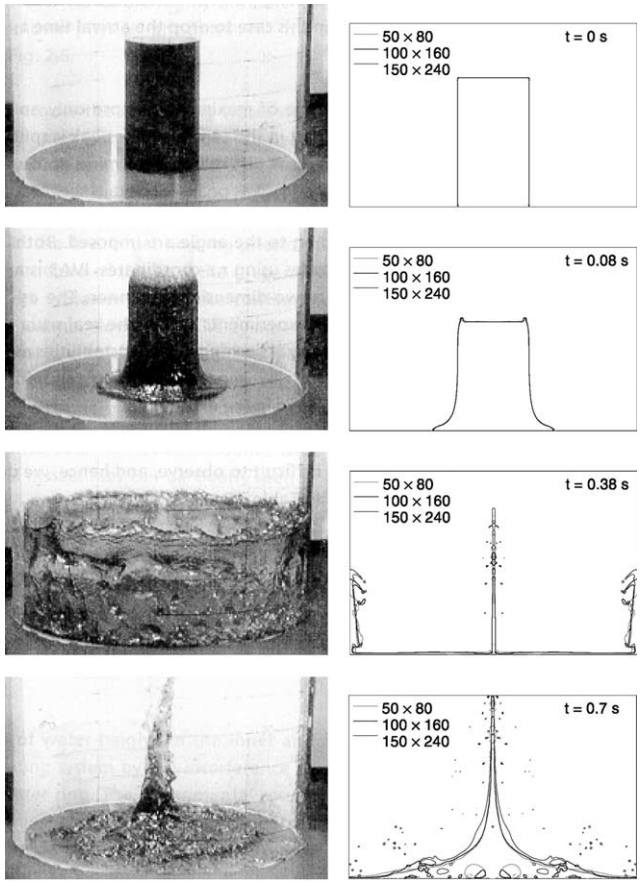

Fig. 5. Movie images of the collapsing cylinder of water from Munz and Maschek (1992), and the corresponding, reconstructed interfaces of PLIC–VOF simulations of Meier (1999). Results of various grid resolutions at different time steps.

4.2.2. Downward injection in a water pool

In the containments of boiling water reactors (BWRs) large bubbles may be formed at the exit of vertical, downwards-pointing vents injecting air and mixtures of steam and non-condensibles into a containment water pool. Meier (1999) carried out a series of experiments to observe the behaviour and condensation of such bubbles in downward and upward injections (see, also, Meier et al., 2000 for more details about the experimental set-up). A sensitivity study had previously been carried out focusing on the effect of the feed-pipe length-to-diameter ratio, the injection orientation, the volumetric flow-rate, and the feed-pipe inflow conditions (constant velocity against oscillating velocity). The experiments yielded valuable data and recordings, which were later (Meier et al., 2002) used to validate the PLIC–VOF variant combined with the modified surface tension model CSF-M introduced in Section 2.3 applied to the problem of gas injection. A qualitative comparison between measured and predicted flow referring to isothermal conditions (injection of pure air) is shown in Fig. 6. The simulation was also two-dimensional and axisymmetric, with imposed unsteady flow conditions at the pipe nozzle and imposed hydrostatic pressure from the far field. The injection velocity was not constant because the flow was oscillating with an imposed frequency in the pipe.

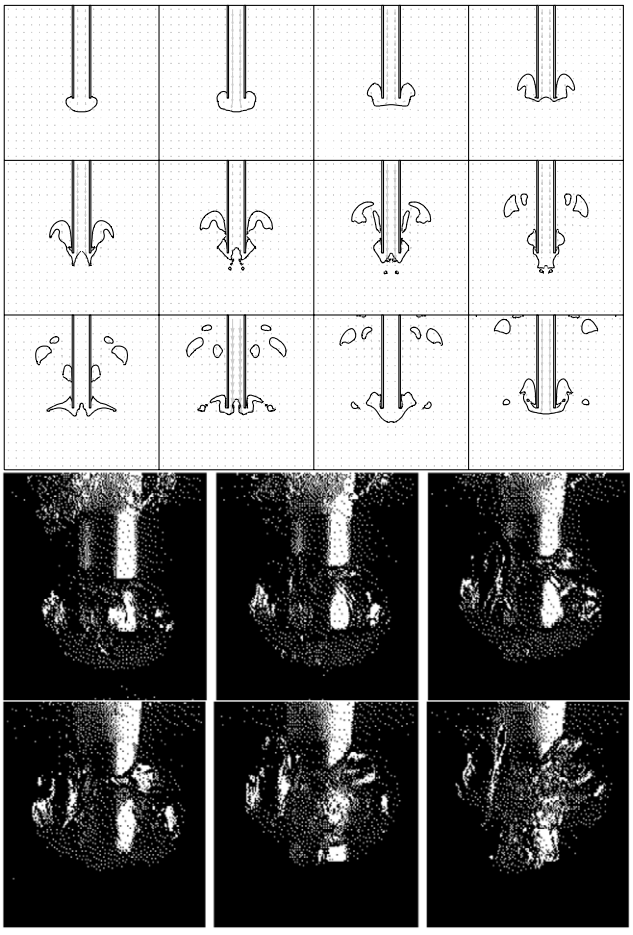

Fig. 6. Bubble formation following injection of air through the downcomer vent. High-speed video images against PLIC–VOF computations (Meier et al., 2000; Meier, 1999). Flow rate of $\dot{V} = 4$ l/s (comp.) and $\dot{V} = 10$ l/s (exp.).

The figure indicates that the model reproduces reasonably well bubble formation, detachment, upward motion, and fragmentation, at least in the early stage of injection during which the flow is still spatially symmetric. Even when the video images shown in Fig. 6 were carefully selected, the axisymmetry of the flow is lost before the bubbles start to rise up away from the nozzle. Frames 1–4 from the upper panel (predictions, upper panel) show the growth of the bubble, frames 6 and 7 are shortly before and after detachment, and frames 8–12 show the breakup of the bubble into many small bubbles. After the detachment of the previous bubble, a new bubble may follow immediately, or the gas may withdraw into the nozzle for a moment and then push out a new bubble. This water intrusion is one of the clues for pressure and velocity oscillations inside the downcomer exit. Note finally that the frequency of the bubbles was also reasonably well predicted in agreement with the data. A summary of the predictions and comparisons can be found in Meier et al. (2000).

5. Level set methods

5.1. Basic formalism

The LS approach (Osher and Sethian, 1988) consists of solving Eq. (1) in a conventional way, while introducing a subtle way for localizing the interface on the grid. The formulation is based on the construction of a smooth function $\phi(\mathbf{x}, t)$, defined everywhere in the computational domain Ω, referring to the shortest distance to the front. Negative values correspond to one of the fluids and positive values to the other. The exact location of the interface $\Gamma(t)$ corresponds to the zero level of ϕ. When expressed in terms of the composition field χ, the LS function is such that $\chi_k = H(\phi)$, where $H(\phi)$ is the Heaviside function defined by

$$H(\phi) = \begin{cases} 1 & \text{if } \phi > 0, \\ 0 & \text{if } \phi < 0. \end{cases} \tag{21}$$

This implies that ϕ_{ij} is directly linked to the *liquid volume fraction* field F_{ij} through

$$F_{ij} = \frac{1}{V} \int_V H[\phi_{ij}] \, \mathrm{d}V. \tag{22}$$

Again, the LS function $\phi(\mathbf{x}, t)$ is governed by the topological Eq. (1). The advantage of using this form of interface tracking first is that it dispenses with interface reconstruction employed in VOF, which are computationally very expensive and difficult (if not impossible) to implement in non-Cartesian configurations. LSs can easily be extended to three dimensions and unstructured meshes. Both methods can handle merging and fragmentation, and permit identification of the exact location of the interface. The disadvantages are interface smearing and non-conservation of mass. In contrast to LSs using an artificial level set function, diffuse-interface models do conserve mass but only when the composition field is defined as a concentration. These will be discussed next.

5.2. Interface thickness relaxation

The LS method is supposed to tackle multiphase flow problems of all sorts, including those involving large ratios of material properties, e.g. $\rho_L/\rho_G > 100$. Sharp variations in density across the interface can be particularly devastating for numerical solvers based on the solution of Poisson equation for the pressure (Fedkiw et al., 1999). In order to relax interfacial changes the interface sublayer is artificially thickened by smoothing some of the physical properties of the fluids, primarily the density, and, when appropriate, the quantities entering into the equations of state, such as the coefficients of thermal expansion and specific heat for the liquid phase.

For that purpose a modified Heaviside function denoted by $\overline{H}(\phi)$ is employed to smooth the physical properties across an interface thickness of 2δ, where δ is typically covered by 1 to 2 cells on each side of the interface (Sussman and Smereka, 1997)

$$\eta(\phi,t)=\eta_{\mathrm{G}}+(\eta_{\mathrm{L}}-\eta_{\mathrm{G}})\overline{H}(\phi), \tag{23}$$

where

$$\overline{H}(\phi)=\begin{cases}0 & \text{if } \phi<-\delta,\\ 1+\frac{\phi}{\delta}+\frac{1}{\pi}\sin\left(\frac{\pi\phi}{\delta}\right) & \text{if } |\phi|\leqslant\delta,\\ 1 & \text{if } \phi>\delta.\end{cases} \tag{24}$$

The same modified Heaviside function is concurrently employed to determine the surface tension which, in this context, can also be cast into the form of a volumetric force by reference to the CSF model (17)

$$\sigma\kappa(\phi)\nabla\overline{H}(\phi). \tag{25}$$

To avoid possible instabilities faced when use is made of pressure-correction schemes, Fedkiw et al. (1999) proposed the *ghost-fluid* method, in which the jumps in density and stress at the interface are smoothed in a particular way. Other authors suggest the use of *projection* methods or *two-step fractional time spliting* methods rather than pressure correction schemes. In these algorithms the velocity is first determined from the momentum equations without pressure gradient, then corrected using the Poisson equation for the pressure.

5.3. Interface smearing

As numerical errors often cause the contours of the LS field to deform as the phase moves, a redistancing algorithm is required to regularize the function. This is an inherent disadvantage of the LS approach as compared to other methods. In other words, advecting the initial distance function $\phi(\mathbf{x},0)$ will not be maintained as such when use is made of Eq. (1) advecting the phase field. An extra redistancing algorithm preserving $|\nabla\phi|=1$ around the zero level of ϕ is therefore required (Sussman et al., 1999).

This task constitutes the largest programming effort of the LS methods. The scheme of Sussman et al. (1999) scheme is the one employed most often. It consists of advecting an intermediate equation for a correction field $d(\mathbf{x},t)$ during a period of intermediate time $\tilde{t}$

$$\frac{\partial d}{\partial\tilde{t}}-\mathrm{sgn}(\phi)(1-|\nabla d|)=0;\quad d(\mathbf{x},0)=\phi(\mathbf{x},t) \tag{26}$$

with $\mathrm{sgn}(\phi)=2H(\mathbf{x})-1$ denoting the signum function. The equation is iterated until d becomes a distance function, i.e. until $|\nabla d|=1$. The corrected ϕ-field is then obtained by setting $\phi(\mathbf{x},t)=d(\mathbf{x},\varepsilon)$, where ε is the time elapsed for Eq. (26) to reach convergence. Osher and Fedkiw (2001) report on recent extensions and other related fast methods.

Originally, the algorithm proposed by Sussman et al. (1999) was based on a second order, non-oscillatory ENO scheme for discretizing the convective flux and a second-order Runge–Kutta time marching scheme. A more robust alternative was found by the authors' group by resorting to simpler, first order forward Euler schemes (Meier and Lakehal, 2000). Apart from this, the optimum near-wall treatment to be employed in connection with Eq. (26) was found to consist in extrapolating d and its second derivatives $\partial^2 d/\partial n^2$ at the boundaries.

Some difficulties may, however, be encountered in stabilizing the solution near the boundaries. This can systematically be alleviated by imposing the following criterion:

$$\text{if } \mathrm{sgn}(d(\mathbf{x},\varepsilon))\neq\mathrm{sgn}(\phi(\mathbf{x}))\quad\text{then } d(\mathbf{x},\varepsilon)=0, \tag{27}$$

acting like an "overheat protection" while not affecting the final result.

Fig. 7 shows an example of phase field redistancing applied to the dam-break problem calculated in two dimensions. The left panel clearly shows a typical scenario of the ϕ-isocontours being smeared around the zero level. Iterating Eq. (26) for 10 time steps provides a perfectly redistanced phase field around $\phi=0$, as shown in the neighbouring panel.

5.4. Mass conservation

The main weakness of the LS methods is that they do not assure mass conservation as a result of employing Eq. (24). In this respect, a simple approach referred to as the *global-volume correction* technique has recently been proposed by the authors' group (Meier and Lakehal, 2000), which can be summarized as follows: at (an artificial) time $\tilde{t}$, the volume $V(\mathbf{x},\tilde{t})$ covered by liquid is determined. Then, after each redistancing of ϕ at $\tilde{t}+\Delta\tilde{t}$ a correction, ϕ_{e}, corresponding to the error in volume $V_{\mathrm{e}}(\mathbf{x},\tilde{t}+\Delta\tilde{t})$ is added overall to the computed ϕ_{c} field such that the liquid volume $V(\mathbf{x},\tilde{t}+\Delta\tilde{t})$ is forced to be equal to $V(\mathbf{x},\tilde{t})$. In two dimensions, the relation for the error in mass estimated over the entire computational domain Ω_{ij} is given by

$$V_{\mathrm{e}}(\tilde{t}+\Delta\tilde{t})=\frac{1}{L}\sum_{i,j}\int_{\Omega_{ij}}|H(\phi_{\mathrm{e}}(t))-H(\phi_{\mathrm{c}}(t))|\,\mathrm{d}\mathbf{x}, \tag{28}$$

where $\phi_{\mathrm{e}}(t)$ is the exact solution of the LS function and $\phi_{\mathrm{c}}(t)$ is the computed one. The perimeter of the interface is denoted by L; in three dimensions it would represent the area covered by the thickness of the interface, δ. The correction can be applied repeatedly, with ϕ converging in less than five subiterations. This method was found to provide global volume conservation for large-scale interfacial structures such as the example shown in Fig. 7. It may, however, lead to non-physical behaviour in sit-

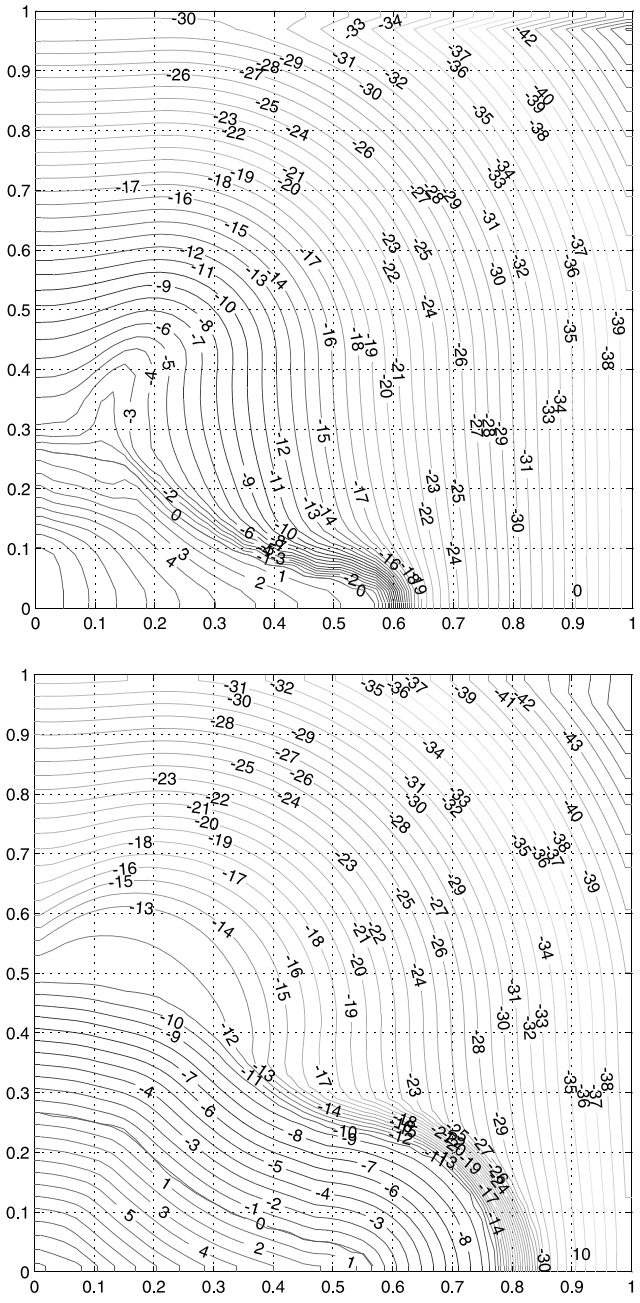

Fig. 7. Example of a LS field in two dimensions, before and after re-initialization (Meier and Lakehal, 2000). The region of correct d propagates, starting from the zero level. At $\tilde{t} = 10\Delta\tilde{t}$, the correct region is about 2×10 cells wide.

uations with small-scale dispersed phases, as in the examples shown in Fig. 1(c).

5.5. Illustrative examples

5.5.1. Rising bubble in a quiescent fluid

The first example simulated by use of LSs is the three-dimensional bubble rising in a quiescent incompressible fluid. The density ratio is of 1000, the viscosity ratio is of 100, and the surface tension coefficient is equal to $\sigma = 0.07$ N/m. The CSF model is employed under the form given by Eq. (25). Fig. 8 shows contours of the signum function $\mathrm{sgn}(\phi)$ applied to the LSs around the bubble. It illustrates the early motion of the bubble at two instants, before the bubble experiences major topology changes.

5.5.2. Gravity driven currents (the lock flow)

Gravity driven currents are induced by density variations due to a difference in temperature, such as atmospheric fronts, or due to the presence of a heavier dispersed phase. These are simple flow configurations, which may, however, result in very complex flows characterized by physical processes such as the emergence of Kelvin–Helmholtz-like instabilities, the formation of lobes and clefts at the front leading edge, etc. This class of flow has only recently been treated by using the one-fluid formulation. Gröbelbauer (1995), for instance, coupled it with the VOF scheme and reported reasonable results only for small to moderate density ratios, up to $\rho_L/\rho_G \approx 20$. Below, we report recent results obtained with LS for the lock flow, [3] where attention was focused on the run-out length and final deposition.

Fig. 9 shows the interface evolution in the lock problem for $\rho_L/\rho_G = 1.38$, where the front intrusions are clearly reproduced. The predicted run-out lengths of the dense and light gas are discussed in the context of Fig. 10, where Gröbelbauer's (1995) VOF results are included for comparison. For almost all gas combinations, the two strategies deliver comparable results. For the gas combination CO_2/argon ($\rho_L/\rho_G = 1.11$) both fronts have nearly equal velocities, in line with Yih's (1965) analytical theory for Boussinesq fronts. For density ratios higher than two (e.g. R22/argon), the dense-gas fronts travel appreciably faster than the fronts of the light gas.

6. The boundary fitting method

6.1. Introductory remarks

As mentioned in the Introduction, combining DNS of turbulence with interface tracking algorithms for predicting turbulent, multiphase flows can only serve as a sophisticated numerical experiment for exploring small-scale phenomena down to the interface. While rigorous DNS of turbulence is generally performed by use of spectral methods (and at low Reynolds numbers only), ITM discussed previously are not precise enough for that task. For this reason another route is required, preferably in the context of the same spectral-based approach.

[3] The lock flow consists of two fluids initially separated by a gate. Mutual intrusion develops after the gate is withdrawn.

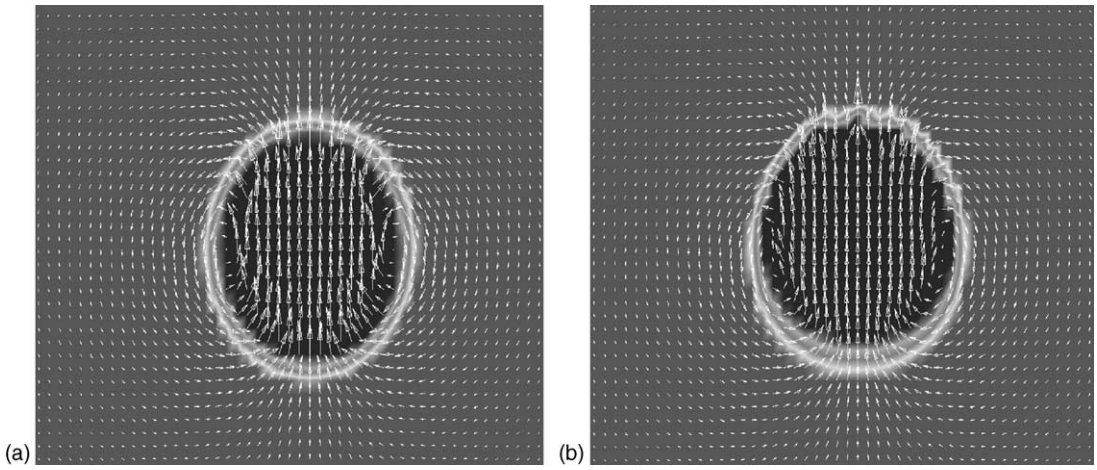

Fig. 8. Flow and interface evolution around a three-dimensional bubble rising in a quiescent fluid for a density ratio of $\rho_L/\rho_G \approx 1000$.

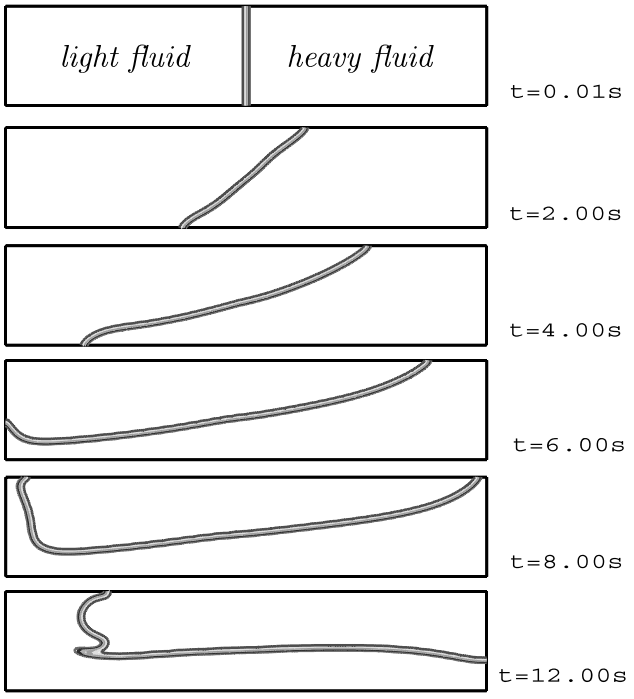

Fig. 9. Interface evolution in the lock flow.

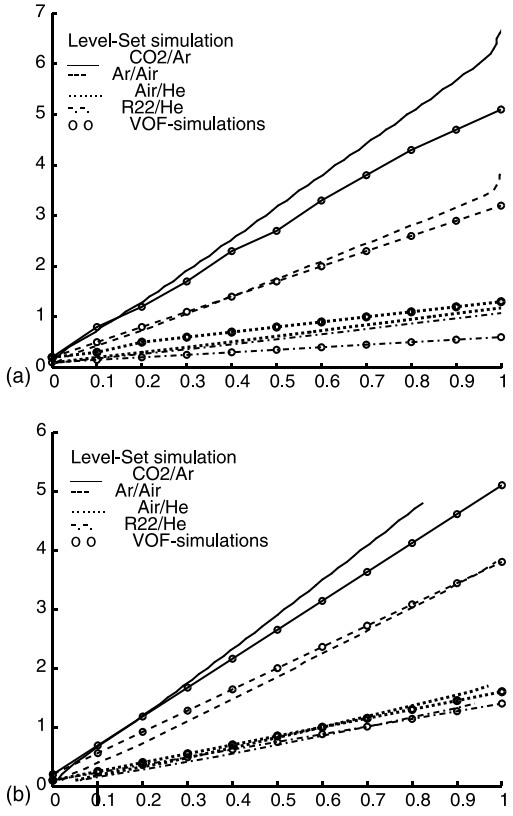

Fig. 10. Front propagation velocities: (a) light gas and (b) dense gas.

Prior to further detailing the method it is perhaps useful to outline the context in which there exists a potential interest for this type of simulation. To summarize, what is not yet fully solved in the direct simulation of multiphase flows is the way ITM can be coupled with turbulence models. For a turbulent flow involving two immiscible, contacting phases the methods may lead to situations where the interface is perceived like a solid surface to one of the phases, a conjecture to which the employed turbulence model needs to conform. The situation can actually be compared to a wall flow where turbulence evolves in a particular way, so that a near-interface low-*Re* turbulence model is necessary. Such a model can be developed by exploiting DNS data of idealized two-phase flows where both turbulence and interface dynamics are free from approximations. This will obviously remain approximative, since high-*Re* number DNS is presently out of reach of available computational resources.

6.2. Description of the method

In the *boundary fitting* method (De Angelis, 1998; Fulgosi et al., 2001), the Navier–Strokes equations with

(constant) material properties defining the fluids present in the system are first solved separately in each subdomain. Subsequently they are coupled explicitly through continuity of velocity and stress jump conditions at the interface. In the absence of heat and mass transfer these jump conditions can be expressed as

$$\begin{aligned}&((\tau_L-\tau_G)\cdot\mathbf{n})\cdot\mathbf{n}+p_G-p_L+\sigma\kappa\nabla\cdot\mathbf{n}\\&\quad+(\rho_L-\rho_G)gf=0,\\&((\tau_L-\tau_G)\cdot\mathbf{n})\cdot t_i=0,\quad i=1,2,\\&\mathbf{u}_G=\mathbf{u}_L,\end{aligned}\tag{29}$$

where t_1 and t_2 denote the two tangential unit vectors at the interface. The interface location has to be identified instantaneously so as to directly impose the jump conditions at the interface. This can be accomplished by transforming Eq. (1) into an equation advecting the vertical elevation of the interface, denoted by $f(\mathbf{x},t)$ around its zero level. In the particular context where the governing equations (including Eq. (1)) are solved using a pseudo-spectral technique the method offers the prospect of a more rigorous strategy than VOF or LS. However, since the equation for interface elevation cannot be extended to strong topological changes, the method remains confined to simple two-phase flow configurations where the topology of the interface is easily definable, like in stratified flows.

6.3. Illustrative example

The example reported here consists of the counter-current air/liquid turbulent shear layer with a deformable interface (see Fulgosi et al., 2001). The grid resolution of each phase was 64^3. The continuity and momentum equations were solved separately in each subdomain, together with Eq. (1) for interface elevation. A pseudo-spectral method was employed. The Reynolds number defined using the effective shear velocity and the half depth of the domain was 85.5 in both phases.

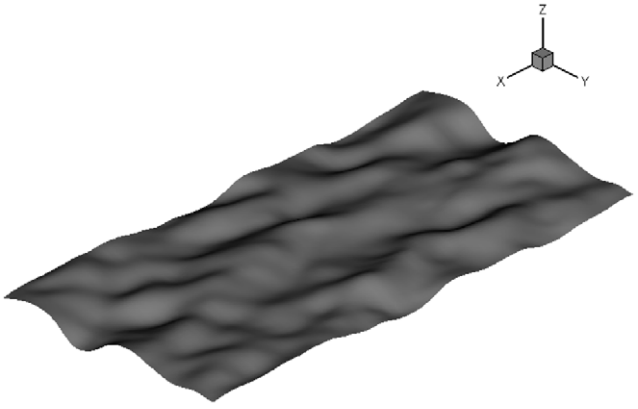

Fig. 11. The topology of the interface separating a counter-current air–water flow.

Since Eq. (1) was solved in the gravity direction only, the method cannot treat strong topological changes such as wave breaking. Thus, parameters reflecting the intensity of surface tension and gravity forces, i.e. the Weber and Froude numbers, were carefully selected so as to limit the elevation amplitude and steepness to the range of capillary waves. Fig. 11 illustrates the topology of the interface at a given time step. Occasionally, flow recirculation between successive crests on the gas side were observed. The major effect expected from interface deformation in the presence of shear is the extra transverse motion superimposed on the mean flow in the direction normal to the interface. Fulgosi et al. (2001)

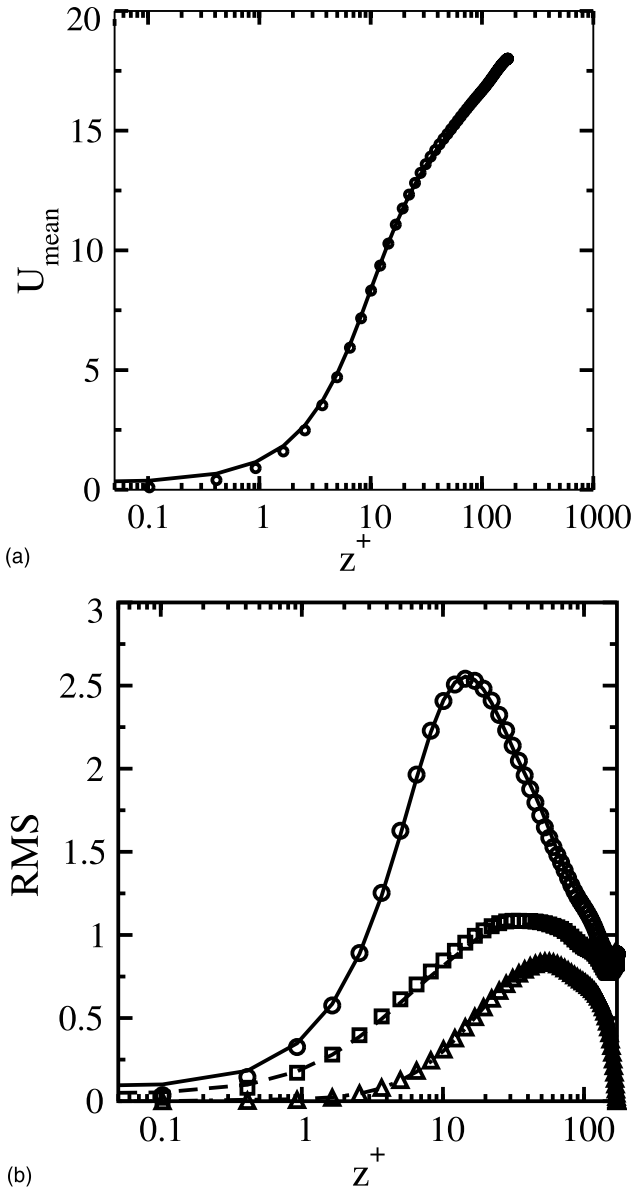

Fig. 12. (a) Profile of the mean streamwise velocity. Lines and symbols are used to identify FDI and OCH, respectively. (b) RMS profiles of the three velocity components. (—) and (○), streamwise velocity; (– – –) and (□), spanwise component; (–·–·–) and (△), normal component.

analyzed this behaviour in detail by comparing their results with available open channel (OCH) flow data.

The way the lighter phase behaves at the interface was examined by looking at the velocity profiles and turbulence structure. Fig. 12 shows the profiles of the mean streamwise velocity for the flow over the deformable interface (FDI) and for the OCH. The velocity profiles are virtually the same except that the origin in the FDI case does not start from zero because of the applied boundary conditions. Fig. 12 shows the RMS profiles of the velocity fluctuations. The behaviour is quasi-identical but again, because of different boundary conditions, the RMS values of u and v in the FDI case do not originate at the same location. The strong similarity in the fluctuating velocities confirms the fact that the gas phase perceives the interface almost like a solid wall. This exercise has the merit of demonstrating the necessity of adapting turbulence models at the interface when employed in connection with direct interface tracking schemes.

7. Inter-phase heat and mass transfer

Mass transfer between gaseous and liquid phases occurs under various conditions. The absorption of slightly soluble gases across an interfacial sublayer differs substantially from strong interfacial mass-suction due to condensation or vaporization. Such phenomena are present in a certain class of nuclear engineering applications like the venting of mixtures of steam and non-condensible gases in containment water pools (see, for example, Fig. 6).

The numerical simulation of interfacial phase change is facing difficulties inherent to the physics of the problem itself. For example, for Prandtl and Schmidt numbers typical of nuclear engineering applications the thickness of regions over which concentration and temperature gradients are significant is only a fraction of a millimeter. Since the rate of mass transfer due to condensation depends on the gradients of mass concentration and temperature across the interface, its determination requires an accurate resolution at the interface. This is obviously not plausible in practical situations. Future research must thus rely on experimental correlations for these transfer mechanisms, or on DNS data, at least for low-to-medium mass fluxes.

Liquid–vapour phase change effects have been resolved within the *one-fluid* formulation by different researchers: Beux et al. (1998) and Son et al. (1999) used the the LS method, Juric and Tryggvason (1998) employed their FT approach, and Jamet et al. (2001) applied the so-called *second gradient* theory or the Cahn–Hilliard equations.

In principle, incorporating heat exchange within the *one-fluid* formulation requires the use of mass and energy jump conditions (Carey, 1992) at the interface defined by

$$\dot{m} = \rho_{\mathrm{L}}(\mathbf{u}_{\mathrm{L}} - \mathbf{V}_{\mathrm{f}}) \cdot \mathbf{n} = \rho_{\mathrm{G}}(\mathbf{u}_{\mathrm{G}} - \mathbf{V}_{\mathbf{f}}) \cdot \mathbf{n} \tag{30}$$

and

$$\dot{m} H_{\mathrm{LG}} + \dot{q} = 0; \quad \dot{q} = (\mathbf{q}_{\mathrm{G}} - \mathbf{q}_{\mathrm{L}}) \cdot \mathbf{n} \tag{31}$$

where $\dot{m}$ is the inter-phase mass flux, H_{LG} is the latent heat of vaporization, $\dot{q}$ is the rate of heat release at the interface, and $\mathbf{V}_{\mathrm{f}}$ is the speed of the front (Fig. 13).

In this instance the mass conservation Eqs. (4) and (5) take the form

$$\frac{\partial}{\partial t}(\chi_{\mathrm{L}}\rho_{\mathrm{L}}) + \nabla \cdot (\chi_{\mathrm{L}}\rho_{\mathrm{L}}\mathbf{u}) = \rho_{\mathrm{L}}(\mathbf{u} - \mathbf{V}_{\mathrm{f}}) \cdot \nabla\chi_{\mathrm{L}}, \tag{32}$$

$$\frac{\partial}{\partial t}[(1-\chi_{\mathrm{L}})\rho_{\mathrm{G}}] + \nabla \cdot [(1-\chi_{\mathrm{L}})\rho_{\mathrm{G}}\mathbf{u}) = -\rho_{\mathrm{G}}(\mathbf{u} - \mathbf{V}_{\mathrm{f}}) \cdot \nabla\chi_{\mathrm{L}}. \tag{33}$$

Summing up these relations and considering the incompressibility of each phase leads to

$$(\rho_{\mathrm{L}} - \rho_{\mathrm{G}})\frac{\mathrm{D}\chi_{\mathrm{L}}}{\mathrm{D}t} + \rho\nabla \cdot \mathbf{u} = (\rho_{\mathrm{L}} - \rho_{\mathrm{G}})(\mathbf{u} - \mathbf{V}_{\mathrm{f}}) \cdot \nabla\chi_{\mathrm{L}}. \tag{34}$$

The above equation can again be split into a pure mass conservation equation, $\nabla \cdot \mathbf{u} = 0$, and a complementary counterpart represented by the topological equation

$$\frac{\partial\chi_{\mathrm{L}}}{\partial t} + \mathbf{u} \cdot \nabla\chi_{\mathrm{L}} = (\mathbf{u} - \mathbf{V}_{\mathrm{f}}) \cdot \nabla\chi_{\mathrm{L}} \tag{35}$$

in which inter-phase mass transfer is reflected by the presence of the source term.

In a typical application of VOF, where χ represents the VOF F_{ij}, Eq. (35) can be rewritten as

$$\frac{\partial F}{\partial t} + \mathbf{u} \cdot \nabla F = \frac{1}{\rho}\int \dot{m}\delta(\mathbf{x} - \mathbf{x}_{\mathbf{f}})\,\mathrm{d}s, \tag{36}$$

where we have used the expression for the jump in mass, Eq. (30), and that of $\nabla\chi$ given by Eq. (18). Next, using the expression for the heat release $\dot{m} = \dot{q}/H_{\mathrm{LG}}$ reduces Eq. (36) to

$$\frac{\partial F}{\partial t} + \mathbf{u} \cdot \nabla F = \frac{1}{\rho H_{\mathrm{LG}}}\int (\mathbf{q}_{\mathrm{G}} - \mathbf{q}_{\mathrm{L}}) \cdot \mathbf{n}\delta(\mathbf{x} - \mathbf{x}_{\mathbf{f}})\,\mathrm{d}s, \tag{37}$$

where the jump in energy $\mathbf{q}_{\mathrm{G}} - \mathbf{q}_{\mathrm{L}}$ can be determined by solving the temperature gradients on both sides of the interface, e.g. $\mathbf{q}_{\mathrm{G}} = -\lambda_{\mathrm{G}}\nabla T|_{\mathrm{G}}$.

In the LS method, where χ is expressed in terms of the distance to the interface ϕ_{ij}, Eq. (35) can be shown to take the form

$$\frac{\partial\phi}{\partial t} + \mathbf{u} \cdot \nabla\phi = \frac{\dot{m}}{\rho}|\nabla\phi|, \tag{38}$$

where, again, use was made of Eq. (30) together with the expression for the normal unit vector $\mathbf{n} = \nabla\phi/|\nabla\phi|$. Inferring next the mass flux $\dot{m}$ from Eq. (31) results in

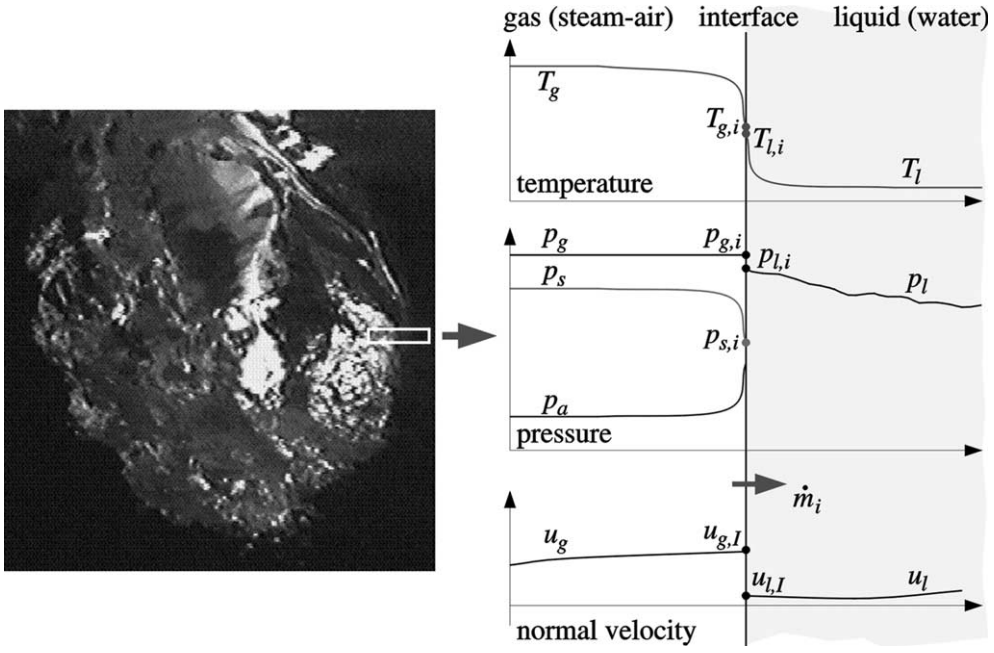

Fig. 13. (Left) schematic of a typical problem with interfacial transfer (downward steam-air injection into water (Meier et al., 2000)); (right) enlarged view of the interfacial region with the inter-phase jump in mass and energy.

$$\frac{\partial \phi}{\partial t} + \mathbf{u} \cdot \nabla \phi = \frac{1}{\rho H_{\mathrm{LG}}} (\mathbf{q}_{\mathrm{G}} - \mathbf{q}_{\mathrm{L}}) \cdot \nabla \phi, \tag{39}$$

which, by use of the modified Heaviside function simplifies to

$$\frac{\partial \phi}{\partial t} + \mathbf{u} \cdot \nabla \phi = \frac{\delta(\phi)}{\rho H_{\mathrm{LG}}} (\mathbf{q}_{\mathrm{G}} - \mathbf{q}_{\mathrm{L}}) \cdot \nabla \overline{H}(\phi). \tag{40}$$

This method was already tested and found to perform reasonably well for low mass fluxes, for example for bubble collapse in a subcooled liquid (Beux et al., 1998), and for nucleate boiling on a horizontal surface (Son et al., 1999). The advantage in this context is that the temperature gradients appearing in Eq. (40) are explicitly expressed in terms of the distance to the interface ϕ. However, the inability of LSs to conserve mass may affect the results.

Within the FT framework, Juric and Tryggvason (1998) proposed solving the topological equation for the front motion in the simplest form given by Eq. (1), and to transform the term on the right-hand side of Eq. (35) to a source of mass resulting from vaporization or condensation. This alternative was also employed by Welch and Wilson (2000) for the prediction of horizontal film boiling in conjunction with one of the VOF variants.

8. Concluding remarks

The paper presents some progress achieved by the authors' group and the recent trends of other researchers in the development of prediction methods for multiphase flows based on the DNS of interface dynamics and inter-phase heat and mass transfer. The paper introduces a generalized form of *one-fluid* formulation based on the evolution of the composition field χ. The strategy does not require further closure relationships for the interfacial area and inter-phase momentum interactions, such as in the classical *two-fluid* method. The χ-based description of the *one-fluid* formulation was used as departure point for other existing methods: The composition field can be manipulated and transformed into the liquid volume fraction F_{ij} in VOF, into the smoothed distance to the interface ϕ_{ij} in LS, or into the vertical elevation f_{ij} in the boundary fitting method. The introduction of capillary forces into the Navier–Stokes equations was also treated in a general way, based on the phase indicator function χ. Other available approaches were also discussed, in particular the assumptions under which the most common form of capillary forces, i.e. the surface tension, can be derived from the basic theory of the free energy density of fluids. Integrating inter-phase heat and mass transfer within the ITM framework has also been examined, and the various possible implementations were discussed departing from the generalized χ-based description.

Some of the challenges to future applications of the VOF and LS methods have been investigated. Their strengths and weaknesses were highlighted and possible orientations were provided via different examples drawn from current work of the authors. The LS method in particular has in fact been shown to be of limited applicability due to its inherent inability to conserve mass.

Available remedies were suggested and simple but limited correction schemes were introduced, such as the *global-mass conservation* algorithm. The VOF approach together with the FT scheme are certainly more precise than LSs, even if their extension to more complex, three-dimensional topology changes still pose serious challenges. A related novel approach referred to as the boundary fitting method was introduced. This *super DNS of multiphase flows* was shown to be a potential experimentation tool for exploring near-interface turbulence structure and related inter-phase heat and mass transfer mechanisms.

Acknowledgements

The authors would like to thank Prof. G. Yadigaroglu and Dr. B. Smith (Paul Scherrer Institute, Switzerland) for their contribution to this work, and J. Davis and Dr. P. Liovic for their valuable comments. The authors express their gratitude to Dr. R. Scardovelli (University of Bologna, Italy) who kindly accepted to read the manuscript. Some of the computations presented in this paper were performed by Ch. Gjerloev and R. Mezzour while they were affiliated with the group.

References

Anderson, D.M., McFadden, G.B., Wheeler, A.A., 1998. Diffuse interface methods in fluid mechanics. Ann. Rev. Fluid Mech. 30, 139.

Beux, F., Knowlton, B., Banerjee, S., 1998. A three-dimensional level-set method for direct numerical simulation of two-phase flows in variable gravity environments. In: Proceedings of the 4th Microgravity Fluid Physics and Transport Phenomena Conference, Clevland.

Brackbill, J.U., Kothe, D.B., Zemach, C., 1992. A continuum method for modelling surface tension. J. Comp. Phys. 100, 335.

Carey, V.P., 1992. Liquid–Vapor Phase-Change Phenomena. Hemisphere Publishing Corporation, Washington.

Chella, R., Vinals, J., 1996. Mixing of a two-phase fluid by cavity flow. Phys. Rev. E 53/4, 3832.

Clift, R., Grace, J.R., Weber, M.E., 1978. Bubbles, Drops, and Particles. Academic Press, New York.

De Angelis, V., 1998. Numerical investigation and modelling of mass transfer processes at sheared gas–liquid interfaces, Ph.D. Thesis, University of California, Santa Barbara.

Drew, D.A., Passman, S.L., 1999. Theory of Multicomponent Fluids. Springer, New York.

Fedkiw, R.P., Aslam, T., Merriman, B., Osher, S., 1999. A non-oscillatory Eulerian approach to interfaces in multimaterial flows (the ghost fluid method). J. Comp. Phys. 152 (2), 457.

Fulgosi, M., Lakehal, D., Banerjee, S., Yadigaroglu, G., 2001. Direct numerical simulation of turbulence and interfacial dynamics in counter-current air–water flows (Procs. DLES-4). In: Geurts, B.J., Friedrich, R., Métais, O. (Eds.), Direct and Large-Eddy Simulation—IV, ERCOFTAC Series, vol. 8. Kluwer Academic Publishers, Dordrecht, pp. 443–452.

Gröbelbauer, H.P., 1995. Experimental study on the dispersion of instantaneously released dense gas clouds, Ph.D. Thesis, ETH Zurich, Switzerland.

Hirt, C.W., Nichols, B.D., 1981. Volume of fluid (VOF) method for the dynamics of free boundaries. J. Comp. Phys. 39, 201.

Ishii, M., 1975. Thermo-fluid Dynamics Theory of Two-phase Flow. Eyrolles, Paris.

Jacqmin, D., 1999. Calculation of two-phase Navier–Stokes flows using phase-field modelling. J. Comp. Phys. 155, 96.

Jamet, D., Lebaigue, O., Coutris, N., Delhaye, J.M., 2001. The second gradient method for the direct numerical simulation of liquid–vapor flows with phase change. J. Comp. Phys. 169, 624.

Juric, D., Tryggvason, G., 1998. Computations of boiling flows. Int. J. Multiphase Flow 24, 387.

Kataoka, I., 1986. Local instant formulation of two-phase flow. Int. J. Multiphase Flow 12, 745.

Kothe, D.B., Mjolsness, R.C., 1992. RIPPLE: A new model for incompressible flows with free surfaces. AIAA J. 30/11, 2694.

Kothe, D.B., Rider, W.J., Mosso, S.J., Brock, J.I., Hochstein, J.S., 1996. Volume tracking of interfaces having surface tension in two and three dimensions, AIAA Paper 96-0859.

Lafaurie, B., Nardone, C., Sardovelli, R., Zaleski, S., Zanetti, G., 1994. Modelling merging and fragmentation in multiphase flows with SURFER. J. Comp. Phys. 113, 134.

Lowengrub, J., Truskinovsky, L., 1998. Quasi-incompressible Cahn–Hilliard fluids and topological transitions. In: Proc. R. Soc. London Ser. A 454, 2617–2654.

Meier, M., Yadigaroglu, G., Smith, B.L., 2002. A novel technique for including surface tension in PLIC–VOF methods. Eur. J. Mech. B: Fluids 21, 61.

Meier, M., Andreani, M., Smith, B.L., Yadigaroglu, G., 2000. Numerical and experimental study of large steam–air bubbles injected in a water pool. Nucl. Sci. Eng. 133, 363.

Meier, M., 1999. Numerical and experimental study of large steam–air bubbles injected in a water pool, Ph.D. Thesis, ETH Zurich, Diss. ETH no. 13091.

Meier, M., Lakehal, D., 2000. Towards a DNS of multiphase flow, Internal report, LKT-01-00, ETH Zurich.

Morel, C., Goreaud, N., Delhaye, J.M., 1999. The local volumetric interfacial area transport equation: derivation and physical significance. Int. J. Multiphase Flow 25, 1099.

Munz C.D., Maschek, W., 1992. Comparison of results of two-phase fluid dynamics codes and sloshing experiments, Internal report KfK 5091, 1-55, Kernforschungszentrum Karlsruhe.

Nadiga, B.T., Zaleski, S., 1996. Investigation of a two-phase fluid model. Eur. J. Mech. B: Fluids 15/6, 885.

Noh, W., Woodward, P., 1976. Simple line interface method (SLIC). In: van de Vooren, A., Zandbergen, P. (Eds.), Proceedings of the 5th International Conferrence on Fluid Dynamics, Lecture Notes in Physics, vol. 59. Springer, Berlin.

Osher, S., Sethian, J.A., 1988. Fronts propagating with curvature-dependent speed: algorithm based on Hamilton-Jacobi formulations. J. Comp. Phys. 79, 12.

Osher, S., Fedkiw, R.P., 2001. Level set methods: an overview and some recent results. J. Comp. Phys. 169, 463.

Richards, J.R., Beris, A.N., Lenhoff, A.M., 1995. Drop formation in liquid–liquid systems before and after jetting. Phys. Fluids 7, 2617.

Rider, W.J., Kothe, D.B., Mosso, S.J., Cerutti, J., Hochstein, J.S., 1995. Volume tracking of interfaces having surface tension in two and three dimensions, AIAA Paper 95-0699.

Rider, W.J., Kothe, D.B., 1998. Reconstructing volume tracking. J. Comp. Phys. 141, 112.

Scardovelli, R., Zaleski, S., 1999. Direct numerical simulation of free-surface and interfacial flow. Ann. Rev. Fluid Mech. 31, 567.

Son, G., Dhir, V.K., Ramanujapu, N., 1999. Dynamics and heat transfer associated with a single bubble during nucleate boiling on a horizontal surface. J. Heat Transfer 121 (3), 623.

Sussman, M., Smereka, P., 1997. Axisymmetric free boundary problems. J. Fluid Mech. 341, 269.

Sussman, M., Almgren, A.S., Bell, J.B., Colella, P., Howell, L.H., Welcome, M.L., 1999. An adaptive level set approach for incompressible two-phase flows. J. Comp. Phys. 148, 81.

Unverdi, S.O., Tryggvason, G., 1992. A front-tracking method for viscous, incompressible, multi-fluid flows. J. Comput. Phys. 100, 25.

Van der Waals, J.D., 1893. Thermodynamische Theorie der Kapillaritaet unter Voraussetzung stetiger Dichteaenderung. J. Statist. Phys. 20, 197.

Verschueren, M., van de Vosse, F.N., Meijer, H.E.H., 2001. Diffuse-interface modelling of thermocapillary flow instabilities in a Hele-Shaw cell. J. Fluid Mech. 434, 153–166.

Welch, S.W.J., Wilson, J., 2000. A volume of fluid based method for fluid flows with phase change. J. Comp. Phys. 160, 662.

Yih, C.S., 1965. Dynamics of Non-homogeneous Fluids. Macmillan, New York.